Structural differences in cortical shell properties between upper and lower human fibula as described by pQCT serial scans. A biomechanical interpretation.

[1]Gustavo R Cointry, [1]Laura Nocciolino, [2]Alex Ireland, [3]Nicolas M Hall, [3]Andreas Kriechbaumer, [1]José L Ferretti, [3]Jörn Rittweger, [1]Ricardo F Capozza.

[1]Center of P-Ca Metabolism Studies (CEMFoC), National University of Rosario, Rosario, Argentina
[2]School of Healthcare Science, Manchester Metropolitan University, Manchester, UK
[3]Division of Space Physiology, Institute of Aerospace Medicine, German Aerospace Center, Cologne, Germany.

Corresponding Author details: Alex Ireland, School of Healthcare Science, Manchester Metropolitan University, John Dalton Building, Chester Street. Manchester, M1 5GD, United Kingdom. Tel: 0044 161 247 1987, Fax: 0044 161 247 5751, Email: a.ireland@mmu.ac.uk

Conflicts of Interest: None.

ABSTRACT

This study describes the structural features of fibula cortical shell as allowed by serial pQCT scans in 10/10 healthy men and women aged 20-40 years. Indicators of cortical mass (mineral content -BMC-, cross-sectional area -CSA-), mineralization (volumetric BMD, vBMD), design (perimeters, thickness, moments of inertia -MIs-) and strength (Bone Strength Indices, BSIs; polar Strength-Strain Index, pSSI) were determined. All cross-sectional shapes and geometrical or strength indicators suggested a sequence of five different regions along the bone, which would be successively adapted to 1. transmit loads from the articular surface to the cortical shell (near the proximal tibia-fibular joint), 2. favor lateral bending (central part of upper half), 3. resist lateral bending (mid-diaphysis), 4. favor lateral bending again (central part of the lower half), and 5. resist bending/torsion (distal end). Cortical BMC and the cortical/total CSA ratio were higher at the midshaft than at both bone ends ($p<0.001$). However, all MIs, BSIs and pSSI values and the endocortical perimeter/cortical CSA ratio (indicator of the *mechanostat's* ability to re-distribute the available cortical mass) showed a "W-shaped" distribution along the bone, with maximums at the mid-shaft and at both bone's ends (site effect, $p<0.001$). The correlation coefficient (r) of the relationship between MIs (y) and cortical vBMD (x) at each bone site ("distribution/quality" curve that describes the efficiency of distribution of the cortical tissue as a function of the local tissue stiffness) was higher at proximal than distal bone regions ($p<0.001$). The results from the study suggest that human fibula is primarily adapted to resist bending and torsion rather than compression stresses, and that fibula's bending strength is lower at the center of its proximal and distal halves and higher at the mid-shaft and at both bone's ends. This would favor, proximally, the elastic absorption of energy by the attached muscles that rotate or evert the foot, and distally, the widening of the heel joint and the resistance to excessive lateral bending. Results also suggest that biomechanical control of structural stiffness differs between proximal and distal fibula.

Key words: *Fibula; Bone structure; Bone biomechanics; Bone mechanostat; Bone adaptation; Bone architecture.*

INTRODUCTION

The mechanical environments of the human fibula and tibia differ greatly. The tibia is a strong bone designed to translate the *compressive* load of the whole body weight from two horizontal articular surfaces in the knee to a single horizontal surface in the heel, and to support relatively large additional bending and torsion stresses toward the midshaft [1,2]. In contrast, the fibula is a thin bone that is firmly attached, by ligaments, to the proximal tibia and free of weight bearing articular surfaces distally. The medial-proximal diaphysis of the fibula serves as insertion points for a number of muscles, the strongest of which participate in the lateral rotation and eversion of the foot.

Some evidence suggests that the fibula would contribute a substantial fraction to resist axial loading together with the tibia. The total mineral mass of the adult human fibula is about 18%-20% of the whole, tibia-fibula bone mass [6]. After fibula harvesting, the tibia cross-section adapts by enhancing its cross-sectional bone area and moment of inertia and rotating its principal longitudinal axes [7]. However, some reports of the relative contribution of the fibula to resist all uniaxial and torsion or lateral-bending stresses passively induced by foot flexion, rotation, inversion and eversion [1,5,8-14] tend to contradict such simplistic interpretation.

Nevertheless, the fibula is considered one of the most important supporting structures of the leg in Eutherian mammals *as related to their particular mechanical environment* (in particular, the use of the foot) rather than the known inter-species, phylogenetic relationships [8]. In fact, foot movements involve not only the contraction of muscles that insert predominantly on the proximal fibula, but also some passive displacements of the lateral malleolus. Accordingly, the fibula can be proposed to have adapted differently in different species. In predators and hominids it seems to adapt to energy storage in the proximal half, to allow for lateral bending in the upper region of its distal half, and to prevent fracture in the lower region of its distal half, as a function of their particular mechanical environments, rather than to support uniaxial stress. This tomographic study aims to collect some human evidence to support this view and to propose some participation of bone *mechanostat* in the involved biomechanical control of fibula's structural properties.

Peripheral quantitative computed tomography (pQCT) provides indicators of cortical tissue mass and mineralization and of cortical shell design and structural stiffness throughout the human fibula, as well as some significant relationships that determine their biomechanical control at every site studied and along the whole bone.

In long bones, the feedback mechanism, bone *mechanostat* would adapt the spatial distribution of the mineralized tissue to resist bending and torsion through a directional modulation of bone modeling as a function of the magnitude and orientation of the strains induced by usage [15-18]. In adults, this adaptation would result chiefly from changes in the activity of teams of modeling/remodeling cells. The *ability* of the resulting modeling process to modify the cross-sectional design of the bone in a mechanically significant way should depend mostly on the relationship between the amount of endocortical modeling/remodeling surface (endocortical perimeter, EcPm) and the total available cortical bone area (CtA) to be re-distributed (EcPm/CtA ratio). The *efficiency* of bone *mechanostat* (mass and orientation of "modeling drifts" [15]) was shown to be inversely related to tissue stiffness, i.e. to the tissue compliance to be deformed. This relationship can be described by typical, hyperbole-shaped curves obtained by correlating pQCT indicators of bone design related to cortical bone tissue "distribution" such as the cross-sectional moments of inertia related to bending and torsion (MI's, *y*) and of bone tissue "quality" (volumetric cortical BMD, vBMD, *x*) that we coined "distribution/quality" (d/q) curves [19-22]. The d/q curves show that "the higher the compliance of the tissue to deformation, the greater the efficiency of the system to compensate for the natural bone strains" [23-25]. In fact, the d/q curves have described the effects of gender, genetic factors, physical activity, bone-weakening diseases and different treatments on bone *mechanostat* [22,26].

These concepts can be applied to demonstrate that the mechanical adaptation of the whole human fibula to its normal mechanical environment responds to different strength patterns in different ways along the bone, as an evidence of a site-specific behavior of bone *mechanostat*. In this study, we hypothesize that "the cortical structure of the human fibula should reflect the mechanical influences described above, which differ between the upper and lower halves of the bone, governed through the general principles of bone mechano-adaptation" [15-18,27]. To test this hypothesis, we took serial pQCT scans of the whole fibula of healthy men and women to describe its cortical structure and the EcPm/CtA and d/q relationships [25-31] and compared the results obtained in different regions of the bone.

MATERIAL AND METHODS

The study participants

Ten men and ten pre-menopausal women of 20-40 years with a body weight of 78.3 ± 2.9 and 57.4 ± 2.4 kg and a body height of 174.7 ± 3.5 and 163.3 ± 2.1 cm, respectively, were recruited as healthy volunteers. None of them had a history of drinking or smoking habits, fractures, bone diseases or treatments with bone-altering drugs, or was following any systematic plan of physical activity. Every participant gave his/her written informed consent before being included. The study was approved by the *Bioethics Committee, Faculty of Medicine, National University of Rosario, Argentina*.

pQCT Measurements.

An *XCT-2000* scanner *(Stratec, Germany),* software version 5.0, was used to scan the entire right leg of each individual. The radiation dose was about 0.9 μSV per scan (20 μSv for the whole study). The slices were 2.5-mm thick, and the in-plane pixel size was 0.5 mm. A previously reported, computer-aided procedure to serially scan the whole tibia [29] was used to analyze the corresponding length of the adjacent fibula. Leg scans were obtained at every 5% of the leg length from the projection of the tibia-talar joint line and the articular line of the knee. Scans were numbered from S5 (5% site, located 5% of the scanned length proximal to the tibia-talar joint) to S95 (95% site, located 95% of the scanned length proximal to the tibia-talar joint). The device allows for no more than 9 slices per session. Thus, each half of the scanned length of the leg had to be studied separately and the scan at S50 (starting point for scanning the proximal segment of the leg) could not be obtained. The distal end of the fibula (analogously to the tibial malleolus as a distal landmark) could not be scanned below the S5 level. Therefore, a total of 18 scans were obtained per fibula (**Fig 1-a**), and any reference to the studied fibula in this study applies to the described fibula length taken proximally from S5 to S95 as above described. Threshold values for total and cortical bone were selected at 180.0 and 710.0 mg/cm^3, respectively, using the parameters *contmode* 2, *peelmode* 2, and *cortmode* 1. The following indicators were obtained as allowed in every site studied [19].

Bone "mass" indicators.

- *Mineral content of total bone (total BMC)*, in g/cm of slice thickness.
- *Mineral content of cortical bone (cortical BMC)*, in g/cm of slice thickness.
- *Cortical bone area*, in mm^2.

These indicators were studied as such and also normalized by body mass (kg) [30] in order to analyze or rule out the influence of allometric factors in the determination of the observed inter-group differences.

Diaphyseal design indicators.

a. Total bone area, cortical perimeters and thickness

- *Periosteal perimeter*, in mm.
- *Total bone area:* bone area comprised inside the periosteal perimeter, in mm.
- *Endocortical perimeter*, in mm.
- *Cortical thickness:* average thickness of the bone cortex, in mm.
- *Endocortical perimeter/cortical area ratio (EcPm/CtA)*: a derived indicator that associates the bone cell availability close to marrow (EcPm) with the amount of available cortical tissue (CtA) to be eventually re-distributed by directionally-oriented modeling/remodeling mechanisms (modeling drifts addressed by bone *mechanostat*) [15].

b. Indicators of the architectural efficiency of cortical tissue distribution within the bone section

- *Cross-sectional moments of inertia (MI's)*: integrated sums of products of the area of every cortical pixel by its squared perpendicular distance to the neutral axes passing through the center of mass of the bone image, after rotating the axis system until achieving a maximal *y* value, as the perpendicular axis to *x* passing through the center of gravity. The reference axes were the longitudinal axis (polar or torsion MI, pMI); the lateral-medial axis (anterior-posterior (A-P) bending MI, xMI); and the A-P axis (lateral bending MI, yMI), in mm^4.

  In contrast with the above procedure applied to normalize the bone "mass" indicators [30], all MI values were normalized by the product [body mass*tibia length] to adjust for body and bone size as proposed by Ruff [30].

***Bone material "quality" (intrinsic stiffness) indicator** [31].*

Volumetric cortical mineral density (cortical vBMD) = cortical BMC/cortical area, mg/cm^3.

Indicators of bone structural stiffness/strength.

Lateral-bending "Bone Strength Index" (yBSI), defined by the equation (derivation in [32])

$$yBSI = yMI \times cortical\ vBMD$$

Polar (torsion) "Bone Strength-Strain Index" (pSSI), defined by the equation

$$pSSI = \frac{pMI \times cortical\ vBMD}{Rmax \times vBMDmax}$$

Rmax being the distance from the farthest periosteal perimeter point to the center of mass of the bone image; and cortical vBMDmax the theoretically maximal value for cortical vBMD = 1,200 mg/cm^3.

Statistical analyses.

Statistica (StatSoft Inc, USA, 2008) software was used. Means and SE's were calculated for each indicator separately in men and women, and plotted by site. The distribution of all the pQCT indicators throughout the fibula was examined in order to define specific aspects of the adaptation of different regions of the bone as required to demonstrate the proposed hypothesis. Factorial ANOVA of the site-related evolution of the studied indicators along the bone in men and women evaluated the higher-order interactive effect of the two studied groups ("sex effect", related to the inter-group differences in the indicator values) and that of the multiple sites scanned ("site-effect", related to the significance of the slopes of the curves) within selected ranges of sites. The MI values of each scan (y) were also compared with the corresponding cortical vBMD values (x) to obtain the above referred d/q curves for every bone site. The d/q curves were always analyzed after pooling men's and women's data together (as done in a previous study of the human tibia [29]) because of the small number of individuals per group. The statistical adjustment (correlation coefficients, r) of the d/q curves obtained at a given bone site would describe the effectiveness of bone *mechanostat* to control bone design as a function of bone stiffness as required by the stresses naturally supported by bone structure at that site. The r values of the d/q curves calculated for each studied bone scan were plotted *(y)* per bone site *(x)* and adjusted to a Lowess curve for descriptive purposes.

RESULTS

The fibula image was inconsistently observed at S95. Accordingly, the tomographic analysis of the fibula was restricted to S5-S90. The size and shape of fibula scans (**Fig 1-a**) were highly variable from site to site throughout the bone. However, the observed cross-sectional features could be roughly classified into the following five types.

1. At S90 (fibula's head medially attached to the tibia by its anterior and posterior ligaments), the cross-section is rounded and almost filled with trabecular bone. 2. At S70-S85, the sections become elliptic with larger A-P than medial-lateral diameters and progressively decreasing in size. 3. At the central diaphysis (S35-S65), the sections increase slightly in size and adopt a triangular shape with the vertices oriented medially. 4. More distally (S20-S30), the sections become smaller and show again an elliptic shape with larger AP than lateral diameters. 5. From S10 to S20, the sections are again triangular but with their vertices pointing laterally, tending to recover the rounded shape at S5.

The longest diameter of the cross-sections is always the A-P diameter. The angle between this diameter and the sagittal plane is relatively small and varies little between sites (**Fig 1-b**), about 2-7 degrees of medial rotation at S5-S80 and 6-18 degrees of lateral rotation at S85-S90.

Tomographic analysis of bone mass, design, density, and strength

The total BMC values were generally higher at the distal than at the proximal half of the fibula (**Fig 2-a**) and higher in men than in women, especially toward the distal part of the bone. The distribution of total BMC values along the fibula showed relatively higher values at both ends and mid-shaft and lower values at the central part of the distal and proximal halves of the bone (site interaction, $p<0.001$), more evidently in males than in females.

Cortical BMC (**Fig 2-b**) and area (not shown) values were higher at the mid-diaphysis than at both ends of the bone and in the distal (S10-S15) than in the proximal (S80-S85) fibula shaft in both sexes. Men's values were higher than women's, especially in the distal part (S10-S45,about +12.5% to +33.3%, $p<0.0001$; S55-S80, about +5.7% to +12.5%, $p<0.01$). Normalizing the total and cortical BMC data to body mass did not equalize the sex difference, but rather reversed the sex differences such that women's values were significantly greater than those in men ($p<0.001$ throughout the bone). The percent proportion of cortical area to total bone area **(Fig 2-c)** was almost constant (about 61-69%) between S30 and S60 and dropped abruptly to about 45% toward the two ends of the bone, in both groups. The percent contribution of the total fibular BMC to the total BMC of the leg [tibia+fibula] along the bone (free from any allometric association), varied only from 11% to 25% in both sexes.

Periosteal perimeter (**Fig 3-a**) was significantly larger in men than women distally ($p<0.001$), not proximally ($p>0.05$). Endocortical perimeter (**Fig 3-b**) was smaller in women than men throughout the bone. Both perimeters showed a "W-shaped" distribution, more visible for the endocortical perimeter. Cortical thickness (**Fig 3-c**) showed maximal values toward the mid-diaphyses in both sexes, but it was significantly greater in men than in women distally, and significantly larger in women than men proximally. The EcPm/CtA ratio (**Fig 3-d**) showed particularly high values toward both bone ends in both sexes with non-significant sex interaction ($p>0.05$), and slightly higher values in men than women at its central part.

In general, MI values (**Fig 4-a,b**) showed quite visibly the alluded "W-shaped" distribution. They were greatest at the proximal (S5-S10) and distal ends (S85-S90) and at the mid-diaphysis (S35-S55) (site effects, always $p<0.001$), with two visible "pits" in the distribution curves placed approximately at S25 and S70-75 (site effects, $p<0.001$). The depths of the two "pits", taken with reference to the "peak" values at S45, tended to be larger for yMI and pMI than for xMI (graph not shown). All crude MI values were higher for men than women all through, more evidently at the central-distal than at the proximal half of the bone.

These inter-sex differences virtually disappeared after adjustment for bone size (for yMI, see **Fig 4-c)**. While the raw MI's data showed significant sex and site effects, the adjusted data showed only the site-related interaction ($p<0.001$).

The cortical vBMD (**Fig 4-d**) was higher in women than in men. Values tended to decay mildly from S20 to S75 and decayed abruptly from S20 to S10 and from S75 to S85.

The yBSI and pSSI values (**Fig 5-a,b**) varied in parallel with those of the MI's (**Fig 4-a,b,c**), and more clearly for the

yBSI than for the pSSI. Also resembling the behavior of MI data, the higher yBSI and pSSI values in men were assimilated to women's values after adjusting for bone length (data not shown).

Determination of the "distribution /quality" (d/q) relationships.

The d/q relationships (**Fig 5-c**) analyzed for men's and women's data together showed a quite variable degree of statistical adjustment (the selected example shown in **Fig 5-c** corresponds to a highly significant relationship). From absolute values of about 0.6-0.7 at S5-S10, r values dropped to almost zero at S25-S30 (**Fig 5-d**); more proximally, they increased abruptly to more than 0.7 at S45, went again down to about 0.4 at S60-S65, and then increased again up to more than 0.7 at S85.

Factorial ANOVA showed highly significant site-effects on changes of both r coefficients (**Fig 5-d**) and pQCT indicators' values (**Figs 2-4 and 5-a,b**) in men and women ($p<0.001$ in all instances). Importantly, the significant site-related variations of the r coefficients of the d/q curves (**Fig 5-d**) were associated with the significant site-related changes observed in most pQCT indicators in both sexes within the above site ranges, as follows.

1. The decrease of r values from S5 to S25-S30 (**Fig 5-d**) corresponded to increases in cortical BMC (about 30%, **Fig 2-b**), periosteal perimeter (about 10%, **Fig 3-a**) and cortical vBMD (about 9.8% from S-10 to S-20, **Fig 5-a**), and to large decreases in endocortical perimeter (65-75%, **Fig 3-b**), EcPm/CtA ratio (55-63%, **Fig 3-d**), MI's (35-65% for yMI, $p<0.001$; **Fig 4-a**), yBSI (25-35%, **Fig 5-b**) and pSSI (11-12%, **Fig 5-a**).

2. The large improvement in r values between S25-S30 and S45 (to note, S45 was the "peak-value site" for most allometrically-related indicators) corresponded to significant increases in cortical BMC (8-10%), all the MI's (35-50% in yMI), yBSI (30-45%), pSSI (11-12%), and the EcPm/CtA ratio (32%, only for men in this particular case), and a 2-3% decrease in cortical vBMD.

3. The decrease in r values from S45 to S60-S65 coincided with decreases in cortical BMC (12-14%) and EcPm/CtA ratio (13-15%), and decreases in cortical vBMD (3-4%), MI's (30-60% in yMI), yBSI (30-67%) and pSSI (12%, only for men in this case).

4. The increase in r values from S60-65 to S85 corresponded to further decreases in cortical BMC (40-50%), and vBMD (11-14%) and increases in the EcPm/CTA ratio (about 110%), MI's (28-38% in yMI), yBSI (20-30%) and pSSI (7-10% from S75-80 to S90).

Changes in cortical vBMD values were unrelated to variations in r values.

DISCUSSION

This study shows that the fibula, despite its almost constant periosteal circumference along its axis, can be subdivided into five anatomically different regions. The following discussion concerns the tomographic data collected in this study. This suggests a different kind of adaptation for the proximal and distal halves of the fibula, more evident in men than women, far beyond any adaptation to support uniaxial stress, and a relevant role of the biological control of fibula's structural properties to the achievement of that adaptation.

1. Adaptation to bending/torsion rather than compression stresses

The rounded shape of the cross-section and the presence of trabecular bone at S90 suggest an adaptation to transmit the loads from the articular surface to the cortical shell. The elliptic shape and relatively smaller size of the cross-sections at S70-S85, with A-P diameters larger than lateral diameters and closely aligned with the sagittal plane, suggest the development of some compliance to lateral-medial bending (assuming an equivalence between compressive and tensile strength). The triangular shape with vertices pointing medially, probably resulting from the traction from the interosseous ligament, and the slightly enhanced size adopted toward the central diaphysis (S35-S70) would resist lateral bending. The elliptic shape and smaller size of the cross-sections that are re-adopted more distally (S20-30) suggest a second trend of the bone to become compliant to lateral-medial bending. The triangular shape with vertices pointing laterally along the S10-S20 region suggests again a trend to resist lateral bending, now unrelated to the interosseous ligament. The trend to re-adopt a rounded shape with a higher BMC value at S5 suggests an additional adaptation to resist torsion stress. No information was obtained from the ultra-distal, malleolar end of the fibula (situated below tibia-S5). The visible smoothness of the evolution of the angle between A-P diameter and sagittal plane from S45 to S55 discards any interference of re-positioning the leg.

The contribution of the human fibula to support uniaxial loads is affected by its anatomical relationships with the tibia [3,5,7] and the complexity of the usual loading patterns. In fact, a more solid tibia/fibula attachment could be expected if axial load sharing were the fibula's main function. The fibula's contribution to total (tibia + fibula) BMC (a correlate of compression strength if no other kinds of stresses are considered) could be 11-25% in humans, and some authors regard it as negligible [1]. This study shows that, despite the high diversity of fibula structure along its shaft, the cortical/total bone area ratio along most of the fibula diaphysis (S20-S70) was relatively constant (variation within 6 percent points within each sex throughout the bone), in contrast with what was observed in the tibia [29]. Therefore, the reported contribution of 18-20% by the fibula to uniaxial compression in the leg after measuring only two fibula sites [6] is unlikely to completely account for the fibula's mechanical environment [2].

The contribution of cadaveric fibulae to support uniaxial loads has been shown to vary widely with the degree of knee flexion and the position of the foot [5,9-11,13,33] from -8% (traction from the anterior and posterior fibular ligament) to 19% (compression of the lateral malleolus) [13]. Furthermore, increasing the load leads to enhancement of the fibular contribution and a decrease in the traction exerted by the ligaments [34]. At any rate, the large variability of fibula's contribution to support uniaxial stress [13] suggests that the fibular total BMC should *not* be adapted to resist compression/traction loads. Evidence from primates suggests that only a negligible amount of load is transmitted to the ground through the fibula. Instead, the size of the *tibia is* related to the weight transmitted through it [35].

In contrast with what we have observed in the tibia [29], in this study, the total *fibular* BMC varied little throughout the bone. In addition, the adjustment of the linear correlation observed between fibula and tibia cortical areas within the same bone sites of different individuals has been shown to decrease proximally from S14 ($R^2 = 0.52$) to S66 ($R^2 = 0.21$). These observations suggest, beyond any allometric influence, that the variation of fibular total BMC with respect to the tibia is independent of any compensatory mechanism related to bone mass control. Furthermore, the inability of the adjustment of bone mass indicators for body *mass* (as compression stress indicators) to compensate for the sex-related differences in this study suggests that bone compression stress should not be a relevant determinant to fibular mass and volume. In agreement with others [2,36-38], these observations conspire against considering the fibula as a significant contributor to support uniaxial stresses by the leg. They rather suggest that the changes in fibular cortical BMC and other features in this study should have been related to *other kind*s of bone stresses than those supported by the tibia.

This study shows that not only total and cortical bone area, but also the shape of the fibula cross-section (variations of all MI values, especially yMI) varies widely throughout the bone. This suggests that the large variability of the fibula's cross section should reflect a site-specific adaptation to bending/torsion rather than compression/traction

stresses, the former being a property for which bone tissue *distribution* rather than mass should play a significant role. The visual analysis of cross-sections' shapes and the generally clearer differences and associations shown by yMI and pMI than by xMI values suggest that lateral bending and perhaps also torsion [28] should be relevant to the determination of fibula's diaphyseal architecture.

To note, the minimization of the sex-related variance of all the MI values (related to bending or torsion strength) after adjustment for *bone length* contrasts with the lack of compensation for those differences after adjusting the fibular *mass* indicators (related to compression/traction strength) for *body mass*. In addition to confirm the relevance of bone length to MI determination [35], this observation rules out any interference of sex hormones with the determination of sex-related differences between bone mass and design indicators.

Furthermore, in long bones, bending loads are thought to cause higher stress than comparable compression loads [39]. Foot dorsiflexion induces lateral *rotation* and posterior displacement of the distal fibula, and foot rotation/inversion/eversion induce a *lateral flexion* of the fibula [40]. In connection with this discussion, stiffness and strain distributions in bending/torsion in different sites of the human fibula are sensitive to the loaded side (more compliance to lateral bending when loading laterally than medially, and more docility to lateral than medial torsion) [14].

2. Differential adaptation of proximal and distal fibula.

Anatomical adaptations of the fibula in Euterian mammals to their mechanical environment [8,41] have followed four different evolutionary pathways, regardless of any taxonomic consideration, allowing specialization for either fast running (fibula reduced to a minuscule *os malleolaris*), burrowing or swimming (robust, inflexible proximal fibula and distal fibula-tibia union) [8], bouncing and jumping (distal tibio-fibular fusion with a thin, flexible "proximal" fibula), or to move on uneven surfaces (separate tibiae and fibulae articulated distally to allow for fibular rotation) [12], as observed in humans. This suggests that 1. when the range of ankle movement is great, the distal fibula must be adjustable, and 2. the proximal fibula existed mainly as a muscular process [42,43] that could be either strong (firm attachment of muscles) or flexible (energy storage during muscle contraction) [8]. Paradigmatically, cheetahs' fibulae are fused to the tibiae just at the mid-diaphysis by a narrow bone bridge, leaving most of the slender, upper and lower parts of the bone completely free to work (and adapt) as separate, independent bones [8,44].

Accordingly, our data suggests that the structure of the upper and lower parts of the human fibula reflect distinct biomechanical behaviors, far beyond a single adaptation of the whole bone to uniaxial loading. Adaptation to allow for lateral bending in proximal fibula could enhance the bone's ability to store elastic energy during the contractions of the strong muscles that evert and rotate the foot. The same adaptation in the proximal part of the distal fibula (virtually free of strong-muscle insertions in humans) could facilitate the expansion of the heel joint during foot dorsiflexion, eversion and external rotation. The stiffening of the most distal part of the fibula (MI and SSI values, S5-S10) could help *resist* lateral bending as well as torsion, hence reducing the risk of fracture by an *excessive* bending, a feature that could be highly selective. Strikingly, the mid-diaphysis shows a high resistance to lateral bending that could facilitate the independent adaptation of the proximal and distal halves of the bone, resembling the cheetah's case.

Importantly, beyond the natural differences between men and women in all mass-related indicators, the distribution of periosteal and endocortical perimeters and cortical thickness along the bone showed striking sex-related differences. 1. In men, the periosteal perimeter was significantly larger than in women distally but not proximally. 2. Cortical thickness was significantly larger in men than in women distally, and significantly larger in women than men proximally. Reasonably, larger periosteal perimeter values in men than women, as well as smaller endocortical perimeter values in women than men could both be also expected because of known hormonal and muscular differences [45]. Another reason for the sex difference in the proximal fibula may pertain to the Q-angle. While this mainly refers to the angle between the patella, the hip and the line of the femur, it affects the kinetic chain of the leg and may influence the way the force is transmitted through the tibia and how the tibia-fibula interact with one another. However, no endocrine explanation can be derived for the distal vs proximal, sex-related differences in periosteal perimeter and cortical thickness.

3. Biological control of the fibula's structural properties

The Theory of Elasticity cannot deal with the variegated features observed in the cortical fibular structure [46]. Such differences can only be explained by a non-symmetric behavior of bone modeling (oriented by bone *mechanostat*) in tension compared with compression, with some sex-related differences [14,47]. Accordingly, the differences in

the EcPm/CtA ratio and in the significance of the d/q curves throughout the fibula in this study may also reflect distinct, site-specific behaviors of bone *mechanostat* [24,27,48].

The distribution of r coefficients of d/q curves showed two “pits”, in parallel with those of the EcPm/CtA ratio, MI’s, BSI’s and pSSI values (chiefly for lateral bending). This suggests that the achievement of a higher or lower resistance to lateral-medial bending or torsion of different sections of the fibula is related to the *mechanostat*’s ability to react to bone tissue deformability and to the relative availability of modeling cell teams (length of the endocortical perimeter) with respect to the amount of cortical area to be modified. However, the adjustment of the d/q curves was very poor distally (r always below the significance limit, 0.4 in S20-S40), and quite high proximally (r always over 0.4 in S45-S85). This indicates a correspondingly lower and higher dependence of bone modeling orientation concerning bending or torsion (as assessed by the MI’s) upon bone tissue stiffness (as assessed by the cortical vBMD).

This finding allows speculation that the distal and proximal “pits” in the distribution of yMI values should have been achieved in association with *different degrees of efficiency* of bone *mechanostat*. The opposing trends in periosteal circumference and endo-cortical remodeling (indicated by cortical BMD), between proximal and distal fibula, could represent a structural expression (perhaps with some sex-specificity) of this apparently paradoxical behavior of bone *mechanostat*.

This particular behavior of fibula’s geometry along the bone and between sexes suggests that bone modeling responses to loads at the distal half would be less-efficiently oriented by bone *mechanostat* than they are more proximally. In contrast, a strikingly good correspondence between yMI or yBSI and r values of the d/q curves was observed toward the proximal and distal ends of the bone (S5-S25 and S70-S85). Proximally, bone mass would be adapted to resist mostly compression stress close to the upper fibula-tibia joint (which would be only spuriously associated with the MI and yBSI values and the fitness of the d/q curves). Conversely, at the distal end of the fibula, the *mechanostat*-oriented improvement in yMI (and yBSI) could improve the resistance to excessive lateral bending and also torsion, in correspondence with the mechanical usage of the bone.

The different adjustment of the d/q curves obtained at given bone sites (bone tissue level), and the particular distribution of the correlation coefficients of those curves along the bone (bone organ level) suggest that, rather than mathematical optimization rules for bone architecture, there seems to be just a biological process which adapts bone structure to mechanical demands, adequate for evolutionary endurance [16,27]. Following this interpretation, the goal of the bone *mechanostat* could be the control of the elastic energy stored locally in the bone matrix upon external loading (strain-energy density) [15,27,49]. This can lead the system to change bone structure differently in different bones or in different regions of the same bone, according to the local mechanical environment. Not only the relative availability of modeling-driving osteocytes (EcPm/CtA ratio), but also their morphological adaptation to strain sensing could be involved in the related mechanisms [50]. This further supports the idea that the *mechanostat* function could also adapt to different types of strains in different skeletal or bone regions at the cellular level of biological organization [27,51-54]. This speculation, if verified, could help understand the different adaptations of the same *mechanostat* system in the human upper and lower fibula to allow for or to resist lateral bending showing different degrees of efficiency, as described here, as a function of the mechanical usage of the bone.

CONCLUSIONS

This study provides an original description of the fibula as allowed by serial pQCT scanning. Results show different adaptations to the mechanical environment in the proximal and distal halves of the bone, chiefly concerning lateral bending or torsion, with only a minor influence of uniaxial stress, that were free of allometric or sex-hormone interactions.

The proximal half of the bone could be adapted to allow lateral bending, presumably as a resource to store elastic energy by the muscles inserted on that region that rotate or evert the foot. The distal half would be adapted, proximally, to allow for lateral bending as needed to permit the passive deformation of the bone resulting from the displacement of the heel joint elements during foot external rotation or eversion; and distally, to resist any excess of that kind of deformation in order to avoid fracture. The central part of the diaphysis, being particularly stiff, should contribute to the manifestation of independent behaviors of the upper and lower halves of the bone.

Within the paradigm of the *Mechanostat* Theory, the output of the system could be adapted differently throughout the fibula to either enhance or reduce the bone structural stiffness as a function of the mechanical usage.

ACKNOWLEDGEMENTS

This study was supported by grants PICT 2012/2810, National Ministry of Science & Technology (MinCyT) and PICT 0475/2010, Argentine National Research Council (CONICET). Drs JLF, GRC and RFC are Members of the Research Career, CONICET. Dr JLF is a Member of the Research Career, Research Council, National University of Rosario, Argentina. Dr LN is a fellowship, MinCyT. Authors are acknowledged to Dr Sara Feldman for providing some of the studied cases.

REFERENCES

01. McNeil CJ, Rayner GH, Doherty TJ, Marsch GD, Rice CL. Geometry of a weight-bearing and non-weight bearing bone in the legs of young, old, and very old men. Calcif Tissue Int 2009; 85:22-30.

02. Rantalainen T, Nikander R, Heinonen A, Sominen H, Sievänen H. Direction-specific diaphyseal geometry and mineral mass distribution of tibia and fibula: a pQCT study of female athletes representing different exercise loading types. Calcif Tissue Int 2010; 86:447-54.

03. Pecina M, Ruszowsky I, Muftic O, Anticevic D. The fibula in clinical and experimental evaluation of the theory on functional adaptation of the bone. Coll Anthropol 1982; 2:197-206.

04. Thomas KA, Harris MB, Willis MC, Lu Y, MacEwen GD. The effects of interosseous membrane and partial fibulectomy on loading of the tibia: a biomechanical study. Orthopedics 1995: 18:373-83.

05. Wang Q, Whittle M, Cunningham J, Kenwright J. Fibula and its ligaments in load transmission and ankle joint stability. Clin Orthop 1996; 330:261-70.

06. Alho A, Höiseth A. Bone mass distribution in the lower leg. A quantitative computed tomographic study of 36 individuals. Acta Orthop Scand 1991; 62:468-70.

07. Taddei F, Balestri M, Rimondi E, Viceconti M, Manfrini M. Tibia adaptation after fibula harvesting. Clin Orthop Relat Res 2009; 467:2149-58.

08. Barnett CH, Napier JR. The rotatory mobility of the fibula in eutherian mammals. J Anat 1953; 87:11-21.

09. Lambert KL. The weight-bearing function of the fibula. J Bone Jt Surg 1971; 73A:507-13.

10. Takebe K, Nakagawa A, Minami H, Kanazawa H, Kirohata K. Role of the fibula in weight-bearing. Clin Orthop 1984; 184:289-92.

11. Goh JC, Mech AM, Lee EH, Ang EJ, Bayon P, Pho RW. Biomechanical study of the load-bearing characteristics of the fibula and the effects of fibular resection. Clin Orthop Relat Res 1992; 279:223-8.

12. Beumer A, Valstar ER, Garling EH, Niesing R, Ranstam J, Löfvenberg R, Swierstra BA. Kinematics of the distal tibiofibular syndesmosis. Acta Orthop Scand 2003; 74:337-43.

13. Funk JR, Rudd RW, Kerrigan JR, Crandall JR. The line of action in the tibia during axial compression of the leg. J Biomech 2007; 40:2277-82.

14. Cristofolini L, Conti G, Juszczyk M, Cremonini S, Van Sint Jan S, Viceconti M. Structural behavior and strain distribution of the long bones of the human lower limbs. J Biomech 2010; 43:826-35.

15. Frost HM (Ed). The Utah Paradigm of Skeletal Physiology. Athens: ISMNI, 2002.

16. Pearson OM, Lieberman DE. The aging of Wolf's "Law": Ontogeny and responses to mechanical loading in cortical bone. Yearb Phys Anthropol 2004; 47:63-99.

17. Hughes JM, Petit MA. Biological underpinnings of Frost's mechanostat thresholds: The important role of osteocytes. J Musculoskel Neuronal Interact 2010; 10:128-35.

18. Ireland A, Maden-Wilkinson T, McPhee J, Cooke K, Narici M, Degens H, Rittweger J. Upper limb muscle-bone asymmetries and bone adaptation in elite youth tennis players. Med Si Sports Exerc 2013; 45:1749-58.

19. Ferretti JL. Peripheral quantitative computed tomography for evaluating structural and mechanical properties of small bone. In: Mechanical Testing of Bone and the Bone-Implant Interface. An YH, Draughn RA (eds). Boca

Raton (FL): CRC Press; 2000, pp 385-405.

20. Ferretti JL, Capozza RF, Mondelo N, Montuori E, Zanchetta JR. Determination of femur structural properties by geometric and material variables as a function of body weight in rats. Evidence of a sexual dimorphism. Bone 1993; 14:265-70.

21. Ferretti JL, Cointry GR, Capozza RF, Frost HM. Bone mass, bone strength, muscle-bone interactions, osteopenias and osteoporoses. Mech Ageing Devel 2003; 124:269-79.

22. Capozza RF, Rittweger J, Reina PS, Mortarino P, Nocciolino LM, Feldman S, Ferretti JL, Cointry GR. pQCT-assessed relationships between diaphyseal design and cortical bone mass and density in the tibiae of healthy sedentary and trained men and women. J Musculoskel Neuron Interact 2013; 13:195-205.

23. Lazenby R. Porosity-geometry interaction in the conservation of bone strength. J Biomech 1986; 19:257-8.

24. Harrington MA Jr, Keller TS, Seiler JG III, Weikert DR, Moeljanto E, Schwartz HS. Geometric properties and the predicted mechanical behavior of adult human clavicles. J Biomech 1993; 26: 417-26.

25. Van Rietbergen B, Odgaard A, Kabeel J, Huiskes R. Relationships between bone morphology and bone elastic properties can be accurately quantified using high-resolution computer reconstructions. J Orthop Res 1998; 16:23-28.

26. Di Masso RJ, Font MT, Capozza RF, Detarsio G, Sosa F, Ferretti JL. Long-bone biomechanics in mice selected for body conformation. Bone 1997; 20:539-45.

27. Huiskes R. If bone is the answer, then what is the question? J Anat 2000; 197:145-56.

28. Mittag U, Kriechbaumer A, Bartsch M, Rittweger J. Form follows function: a computational simulation exercise on bone shape forming and conservation. J Musculoskel Neuron Interact 2015; 15:215-26.

29. Capozza RF, Feldman S, Mortarino P, Reina PS, Schiessl H, Rittweger J, Ferretti JL, Cointry GR. Structural analysis of the human tibia by tomographic (pQCT) serial scans. J Anat 2010; 216:470-81.

30. Ruff CB. Body size, body shape, and long bone strength in modern humans. J Hum Evol 2000; 38:269-90.

31. Currey JD. Incompatible mechanical properties in compact bone. J Theor Biol 2004; 569-80.

32. Ferretti JL, Capozza RF, Zanchetta JR. Mechanical validation of a tomographic (pQCT) index for noninvasive estimation of rat femur bending strength. Bone 1996; 18:97-102.

33. Segal D, Pick RY, Klein HA, Heskiaoff D. The role of lateral malleolus as a stabilizing factor of the ankle joint: preliminary report. Foot Ankle 1981; 2:25-9.

34. Attarian DE, McCrackin HJ, De Vito DP, McElhaney H, Garret WE Jr. Biomechanical characteristics of human ankle ligaments. Foot Ankle 1985; 6:54-8.

35. Reina P, Cointry GR, Nocciolino L, Feldman S, Ferretti JL, Rittweger J, Capozza RF. Analysis of the independent power of age-related, anthropometric and mechanical factors as determinants of the structure of radius and tibia in normal adults. A pQCT study. J Musculoskel Neuron Interact 2015; 15:10-22.

36. Campbell B (ed). Human Evolution, 4th Ed. New Jersey: Campbell; 1988.

37. Marchi D. Relative strength of the tibia and fibula and locomotor behavior in hominoids. J Hum Evol 2007; 53:647-55.

38. Rantalainen T, Duckhem RL, Suominen H, Heinonen A, Alén M, Korhonen MT. Tibial and fibular mid-shaft

bone traits in young and older sprinters and non-athletic men. Calcif Tissue Int 2014; 95:132-40.

39. Heinonen A, Sievänen H, Kyröläinen H, Pertunnen J, Kannus P. Mineral mass, size, and estimated mechanical strength of triple jumpers' lower limb. Bone 2001; 29:279-85.

40. Norkus SA, Floyd RT. The anatomy and mechanisms of syndesmotic ankle sprains. J Athl Train 2001; 56:68-73.

41. Marchi D, Shaw CN. Variation on fibular robusticity reflects variation in mobility patterns. J Hum Evol 2011; 61:609-16.

42. Thorpe SKS, Crompton RH, Günther MM, Ker RF, Alexander RM. Dimension and moment arms of the hind- and forelimb muscles of common chimpanzees (*Pan troglodytes*). Am J Phys Anthropol 1999; 110:179-99.

43. McLean SP, Marzke M. Functional significance of the fibula: contrasts between humans and chimpanzees. Folia Primatol 1994; 107-14.

44. Howell AB (ed). Speed in Animals. Chicago: University of Chicago Press; 1944.

45. Lorentzon M, Swanson C, Andersson N, Mellström D, Ohlsson C. Free testosterone is a positive, whereas free estradiol is a negative, predictor of cortical bone size in young Swedish men: The GOOD Study. J Bone Miner Res 2005; 20:1334-41.

46. Timoshenko PS, Godier JN (Eds). Theory of Elasticity. New York: McGraw Hill; 1982.

47. Walmsley T. The reduction of the mammalian fibula. J Anat Lond 1918; 52:326-31.

48. Kuruvilla SJ, Fox SD, Cullen DM, Akhter MP. Site-specific bone adaptation response to mechanical loading. J Musculoskel Neuronal Interact 2008; 8:71-8.

49. Lanyon L. Strain-related control of bone (re)modeling: objectives, mechanisms and failures. J Musculoskel Neuron Interact 2008; 8:298-300

50. Vatsa A, Breuls RG, Semeins CM, Salmon PL, Smit TH, Klein-Nulend J. Osteocyte morphology in fibula and calvaria – Is there a role for mechanosensing? Bone 2008; 43:452-8.

51. Rawlinson SCF, Mosley JR, Suswillo RFL, Pitsillides AA, Lanyon LE. Calvarial and limb bone cells in organ and monolayer culture do not show the same early responses to dynamic mechanical strain. J Bone Miner Res 1995; 10: 1225-32.

52. Buckley K, Kerns JG, Birch HL, Gikas PD, Parker AW, Matousek P, Goodship AE. Functional adaptation of long bone extremities involves the localized "tuning" of the cortical bone composition; evidence from Raman spectroscopy. J Biomed Optics 2014; 19: *DOI: 101.1117/1.JBO.19.11.111602.*

53. Schlecht SH, Bigelow EMR, Jepsen KJ. Mapping the natural variation in whole bone stiffness and strength across skeletal sites. Bone 2014; 67:15-22.

54. Lai X, Price C, Modla S, Thompson WR, Caplan J, Kirn-Safran CB, Wang L. The dependences of osteocyte network on bone compartment, age, and disease. Bone Res 2015; 3. *doi: 10.1038/boneres.2015.9.*

Legends and captions for the figures

Figure 1

a. Caption: ***Typical pQCT scans of the studied sites***

Legend: Scans obtained in the analyzed sites of the studied region of the leg in one of the male individuals. The image corresponding to site S95 (situated 5% distal to the articular knee line) was not analyzed because of the inconstancy of the fibular image at that level. The S50 site (situated at the midshaft) could not be scanned because of technical impediments. Images are shown of scans taken from sites S90 (10% distal the the knee articular line) to S55 (5% proximal to the midpoint of the scanned bone) in the upper row, and from sites S45 (5% distal to that midpoint) to S5 (5% proximal to the heel joint line) in the lower row.

b. Caption: ***Rotation angles of the A-P axis along the fibula***

Legend: Mean of all individual rotation angles of the A-P axis of the fibula images of all individuals together throughout the analyzed region of the leg, from sites S5 (5% proximal to the heel joint line) to S90 (10% distal to the knee joint line).

Figure 2.

Caption: ***Distribution of indicators of bone mass along the fibula***

Legend: Distribution of total BMC **(a)** and cortical BMC values **(b)** and of the percentage of cortical area with respect to the total bone area **(c)** through the fibulae of the analyzed men and women. In (**a**) and (**b**), horizontal lines indicate the ranges of bone sites (described between brackets) within which the intergroup differences were found significant after factorial ANOVA tests; F and p values are indicated for the corresponding intervals. In (**c**), the same analysis gave no significant results within the indicated site range.

Figure 3.

Caption: ***Distribution of indicators of bone diameters along the fibula***

Legend: Distribution of periosteal **(a)** and endocortical **(b)** perimeters, cortical thickness **(c)** and the endocortical perimeter/cortical area ratio (EcPm/CtA) **(d)** throughout the fibulae of the studied men and women. Horizontal lines indicate the ranges of bone sites (described between brackets) within which the intergroup differences were found significant after factorial ANOVA tests; F and p values are indicated for the corresponding intervals. A non-significant but relevant result to the interpretation of the study is indicated analogously at the right side of the graph **(a)**.

Figure 4.

Caption: ***Distribution of moments of inertia and cortical vBMD along the fibula***

Legend: Distribution of crude yMI **(a)**, crude pMI **(b)**, and MI normalized by body mass and bone length (normalized yMI) **(c)**, and cortical vBMD values **(d)** throughout the fibulae of the studied men and women. In **(a)** and **(b)**, horizontal lines indicate the ranges of bone sites (described between brackets) within which the intergroup differences were found significant after factorial ANOVA tests; F and p values are indicated for the corresponding intervals. No significant results were obtained throughout the bone concerning **(c)**.

Figure 5.

Caption: ***Distribution of strength indicators and analysis of the d/q relationships***

Legend: Distribution of yBSI **(a)** and pSSI **(b)** values throughout the fibulae of the studied men and women. Horizontal lines indicate the ranges of bone sites (described between brackets) within which the intergroup differences were found significant after factorial ANOVA tests; F and p values are indicated for the corresponding intervals. **c.** Example of a typical “distribution (crude yMI, *y*) / quality (cortical vBMD, *x*)” relationship (*d/q* curve) calculated for the fibulae of the whole group of men and women together as determined by data taken at the S80

(80%) site. The correlation coefficient (r) and its statistical significance are indicated. **d.** Lowess curve describing the distribution of the r coefficients of the *d/q* relationships calculated for every site studied from S5 to S85 in the fibulae of men and women together as represented in **(c)** for S80.

a

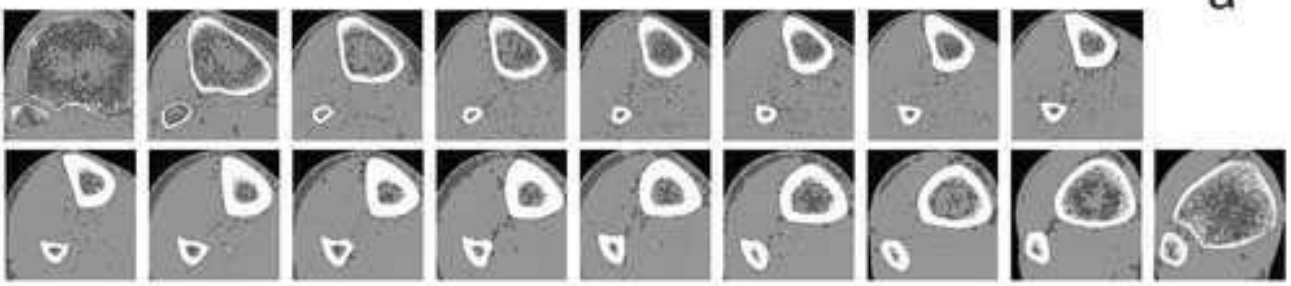

b

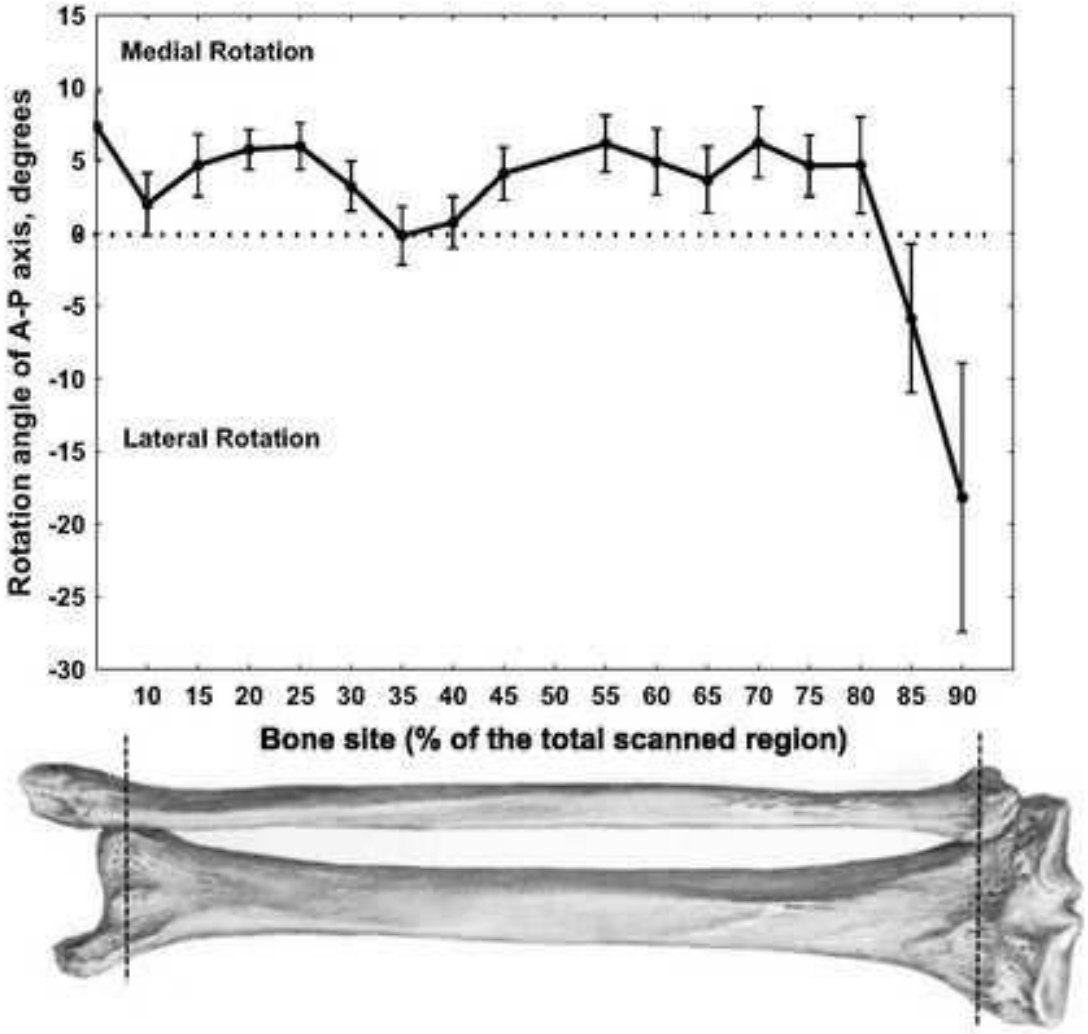
Medial Rotation
Lateral Rotation
Rotation angle of A-P axis, degrees
15
10
5
0
-5
-10
-15
-20
-25
-30
10 15 20 25 30 35 40 45 50 55 60 65 70 75 80 85 90
Bone site (% of the total scanned region)

FIGURE 1

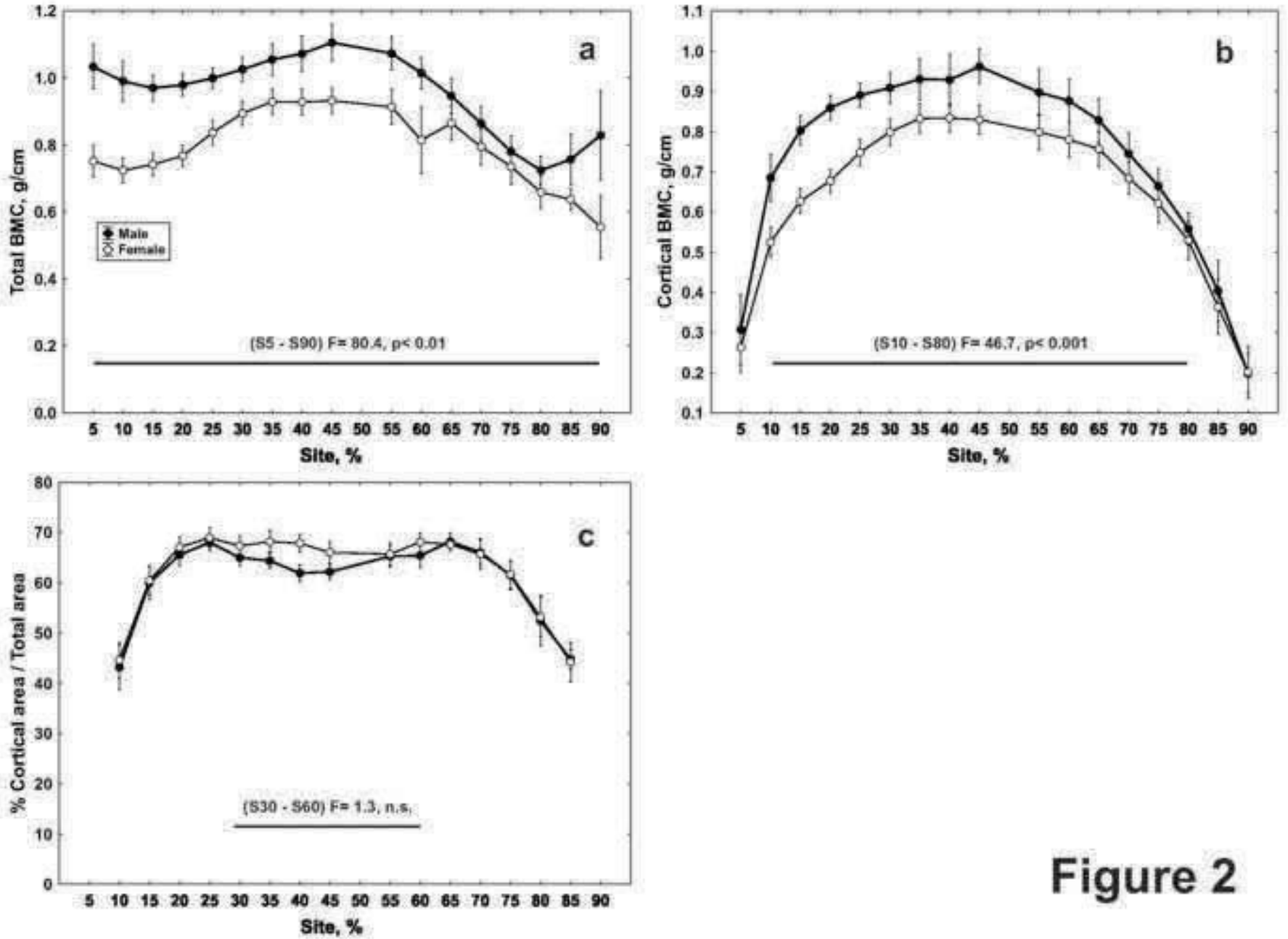
a
Total BMC, g/cm
Male
Female
(S5 - S90) F= 80.4, p< 0.01
Site, %
b
Cortical BMC, g/cm
(S10 - S80) F= 46.7, p< 0.001
Site, %
c
% Cortical area / Total area
(S30 - S60) F= 1.3, n.s.
Site, %

Figure 2

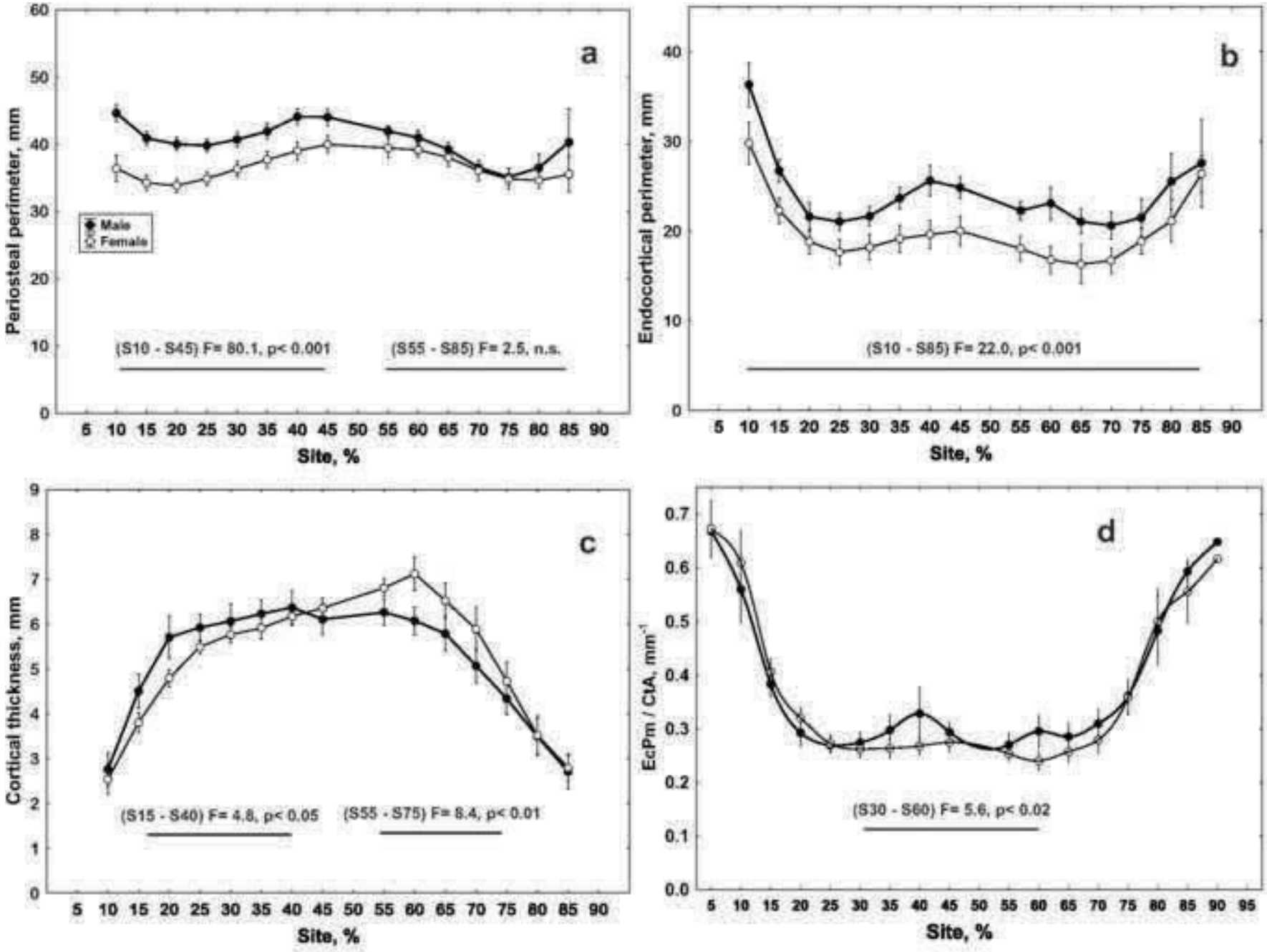
a
Periosteal perimeter, mm
Male
Female
(S10 - S45) F= 80.1, p< 0.001
(S55 - S85) F= 2.5, n.s.
Site, %
b
Endocortical perimeter, mm
(S10 - S85) F= 22.0, p< 0.001
Site, %
c
Cortical thickness, mm
(S15 - S40) F= 4.8, p< 0.05
(S55 - S75) F= 8.4, p< 0.01
Site, %
d
EcPm / CtA, mm-1
(S30 - S60) F= 5.6, p< 0.02
Site, %

Figure 3

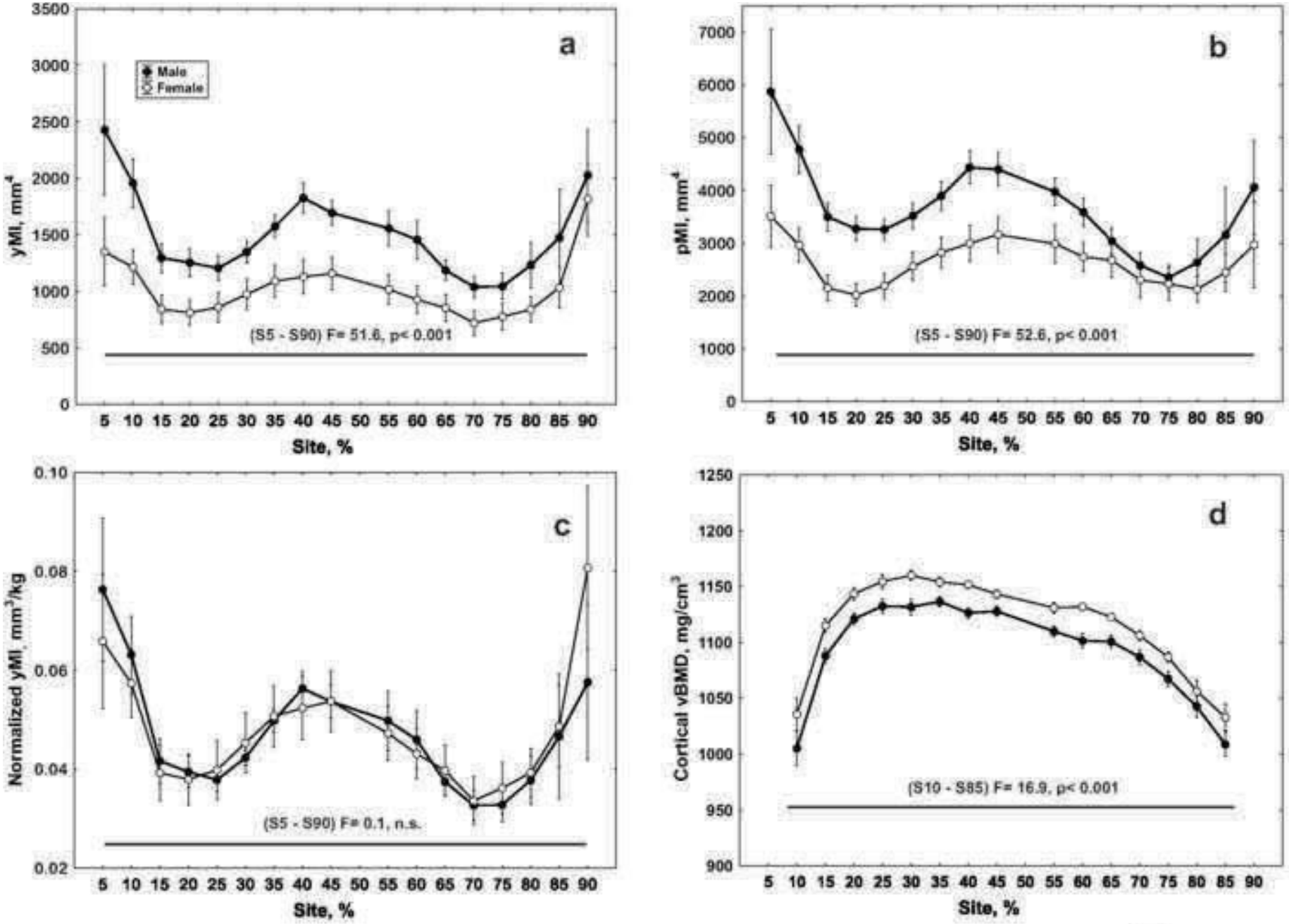
a
Male
Female
yMI, mm4
(S5 - S90) F= 51.6, p< 0.001
Site, %
b
pMI, mm4
(S5 - S90) F= 52.6, p< 0.001
Site, %
c
Normalized yMI, mm3/kg
(S5 - S90) F= 0.1, n.s.
Site, %
d
Cortical vBMD, mg/cm3
(S10 - S85) F= 16.9, p< 0.001
Site, %

Figure 4

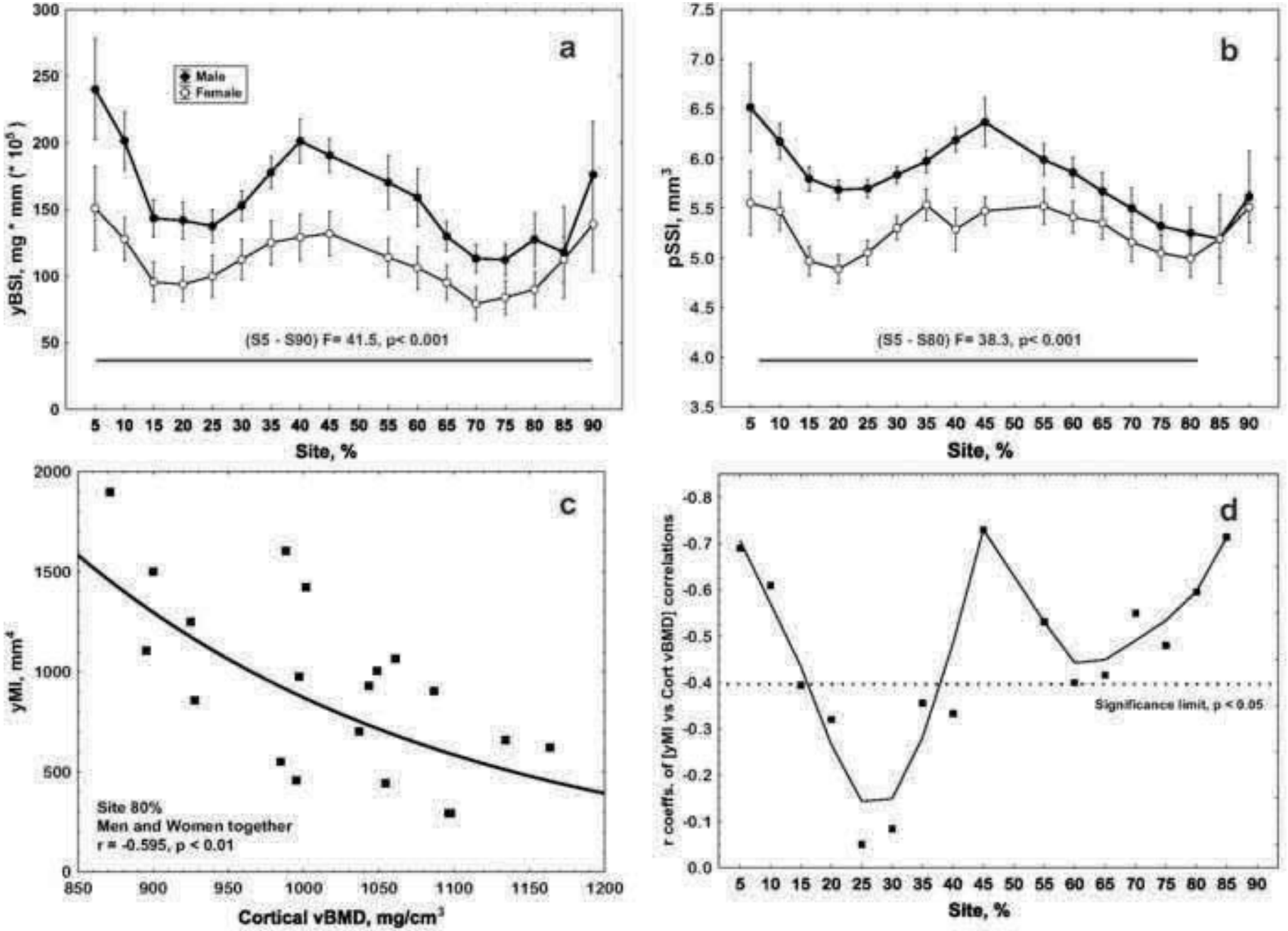
a
Male
Female
yBSI, mg * mm (* 10^5)
(S5 - S90) F= 41.5, p< 0.001
Site, %
b
pSSI, mm^3
(S5 - S80) F= 38.3, p< 0.001
Site, %
c
yMI, mm^4
Site 80%
Men and Women together
r = -0.595, p < 0.01
Cortical vBMD, mg/cm^3
d
r coeffs. of [yMI vs Cort vBMD] correlations
Significance limit, p < 0.05
Site, %

Figure 5